arXiv:1605.02861v1 [hep-ex] 10 May 2016

Chapter 1
A method to measure vacuum birefringence at FCC-ee

Ulrik I. Uggerhøj and Tobias N. Wistisen

Abstract It is well-known that the Heisenberg-Euler-Schwinger effective Lagrangian predicts that a vacuum with a strong static electromagnetic field turns birefringent. We propose a scheme that can be implemented at the planned FCC-ee, to measure the nonlinear effect of vacuum birefringence in electrodynamics arising from QED corrections. Our scheme employs a pulsed laser to create Compton backscattered photons off a high energy electron beam, with the FCC-ee as a particularly interesting example. These photons will pass through a strong static magnetic field, which changes the state of polarization of the radiation - an effect proportional to the photon energy. This change will be measured by the use of an aligned single-crystal, where a large difference in the pair production cross-sections can be achieved. In the proposed experimental setup the birefringence effect gives rise to a difference in the number of pairs created in the analyzing crystal, stemming from the fact that the initial laser light has a varying state of polarization, achieved with a rotating quarter wave plate. Evidence for the vacuum birefringent effect will be seen as a distinct peak in the Fourier transform spectrum of the pair-production rate signal. This tell-tale signal can be significantly above background with only few hours of measurement, in particular at high energies.

1.1 Introduction

In this paper we employ natural units $\hbar = c = 1$, $\alpha = e^2$. The Heisenberg-Euler-Schwinger effective Lagrangian describes the electromagnetic fields while keeping only the QED corrections to lowest order in the fine structure constant, but including any (even) number of photons. The result was

Department of Physics and Astronomy, Aarhus University, Denmark

first derived by W. Heisenberg and H. Euler. [1]. We use the expression of J. Schwinger [2] which has an asymptotic expansion of the Lagrangian:

$$\mathcal{L} = \mathcal{F} + \frac{\alpha^2}{90\pi m^4}\left[4\mathcal{F}^2 + 7\mathcal{G}^2\right] + ..., \tag{1.1}$$

If one considers the situation with two fields, a strong static "background" field, and a weak perturbing radiation field, one can from the above Lagrangian derive the field equations for the radiation field. To leading order in the "background" fields this manifests itself, as if the radiation were propagating in a dielectric medium, with the permittivity and permeability depending on the strong background fields

$$\epsilon_{ik} = \delta_{ik} + \frac{\alpha^2}{45\pi m^4}\left[2(\mathbf{E}^2 - \mathbf{B}^2)\delta_{ik} + 7B_iB_k\right], \tag{1.2}$$

$$\mu_{ik} = \delta_{ik} + \frac{\alpha^2}{45\pi m^4}\left[2(\mathbf{B}^2 - \mathbf{E}^2)\delta_{ik} + 7E_iE_k\right], \tag{1.3}$$

as seen in [3] or [4]. The field quantities in these dielectric tensors are the ones from the strong background field, which we here take as being purely magnetic in the laboratory frame. Solutions are readily obtained which yield a difference in the refractive index, depending on whether the polarization of the radiation is in the same direction as the magnetic field, or perpendicular to it. The results are

$$n_\perp = 1 + \frac{7\alpha}{90\pi}\frac{\mathbf{B}^2}{B_c^2}, \tag{1.4}$$

$$n_\parallel = 1 + \frac{2\alpha}{45\pi}\frac{\mathbf{B}^2}{B_c^2}. \tag{1.5}$$

where $B_c = \frac{m^2}{e}$ is the Schwinger critical field ($4.4 \cdot 10^9$T). Formulas (1.4) and (1.5) are the low frequency limit of the general result [4],[5], valid as long as $\omega \ll m\frac{B_c}{B}$, where B is the strength of the static magnetic background field. Our proposal operates far below this limit. The difference in refractive indices induces a phase shift of the radiation between the two polarization directions given by

$$\Delta = \omega L_B \frac{3\alpha}{90\pi}\frac{\mathbf{B}^2}{B_c^2}, \tag{1.6}$$

with L_B being the length of the dipole magnet and ω the photon energy.

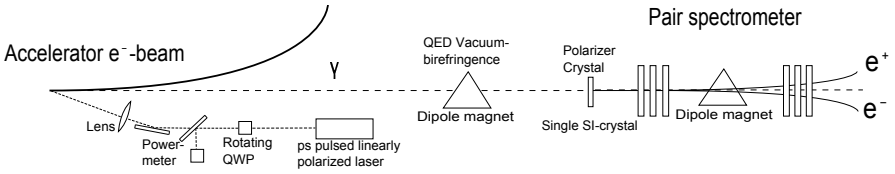

Fig. 1.1 Experimental setup. Linearly polarized laser light passes through a rotating quarter wave-plate, the power is measured from a small fraction of the light, and then the remaining light undergoes Compton backscattering. The backscattered photons pass through the high field dipole magnet, and the resulting radiation is analyzed using a properly oriented single Si-crystal followed by a pair spectrometer.

1.2 Experimental setup

The experimental setup proposed to measure this effect can be seen in figure 1.1. In short, linearly polarized laser light passes through a rotating quarter-wave plate, the power is measured and then the light undergoes Compton backscattering from the intense and energetic electron beam. The electron beam must be of low emittance and short pulse-length where the laser pulse is matched with the duration of the e^--beam. The backscattered photons, now of very high energy, pass through a high field dipole magnet which for this example is taken as a standard LHC dipole, and the resulting radiation is analyzed using a single Si-crystal and a pair spectrometer. The frequency of rotation of the initial quarter-wave plate then gives rise to a distinct peak in the Fourier spectrum of the number of pairs produced – yielding a clear signal of the effect sought.

1.2.1 Electron beam parameters

For the electron beam, we choose the parameters of the FCC-ee as given in [6]. The FCC-ee is a circular machine of circumference 80-100 km which is presently under study, mainly at CERN, and it has several stages named after its main production potential, e.g. the `tt`-stage for top-production. The energies of the stages are 45.5 GeV (`Z`-stage), 80 GeV (`W`-stage), 120 GeV (`H`-stage) and 175 GeV (`tt`-stage).

1.2.2 Modification of the polarization state

To calculate the resulting pair creation rate at the tracking detectors we use the formalism of Müller calculus [7] which facilitates the calculation of the polarization and intensity of radiation through an optical system. The

radiation is described by a Stokes vector and the optical elements with a Müller matrix, for details see [8]. The final Stokes vector is determined by operating on the initial Stokes vector by the Müller matrix of each component of the setup. In our setup, we will have 4 Müller matrices. One for a rotating quarter-wave-plate, one for the Compton backscattering process, one for the QED process and one for the crystal polarizer. Thus, we obtain the intensity in each polarization component.

1.2.3 Compton backscattering

We employ the differential cross section for Compton scattering for the initial polarization state in question, given in [9], which is identical to – but expressed differently from – the Klein-Nishina cross section. Since the Klein-Nishina cross section applies to an electron at rest, two Lorentz-transformations are required to get the backscattering cross section and the emerging photon energies.

1.2.4 Pair production

For the experimental analysis of the polarisation state, we utilize the state-dependent pair production rate from each of the two orthogonal directions in the crystal. The transmittances are given as $\mathcal{T}_\perp = e^{-\sigma_\perp(y)\cdot L}$ and $\mathcal{T}_\parallel = e^{-\sigma_\parallel(y)\cdot L}$ with L being the traversed distance and $\sigma_\perp(y)$, $\sigma_\parallel(y)$ being the total number of pairs created per distance (the inverse of the mean free path), which depend on the photon energy parametrized by $y = \omega_f/E$. To calculate the pair production cross-sections we use the theory of coherent pair production, see e.g. [10]. The differential pair production cross section depends on the asymmetry between the energies of the two particles: $z = \frac{\varepsilon_-}{yE}$, with ε_- being the energy of the pair-produced electron.

The maximum photon energy ω_m of the Compton backscattered photons in the interaction of an electron beam of energy E and a laser with photons of energy ω_0 is given as

$$\omega_m = E\frac{x}{x+1} \qquad \text{with} \qquad x = \frac{4E\omega_0}{m^2} \tag{1.7}$$

which for $E = 175$ GeV and $\lambda_0 = 1064$ nm, i.e. $\omega_0 = 1.165$ eV, yields $x = 3.12$ and thus $\omega_m = 132.5$ GeV. The threshold for creation of pairs is $\omega_0\omega_m = m^2c^4$ which corresponds to $x^2/4(x+1) = 1$ or $x = 2(1+\sqrt{2}) \simeq 4.83$, so our scheme is still below the photon-photon pair-production threshold.

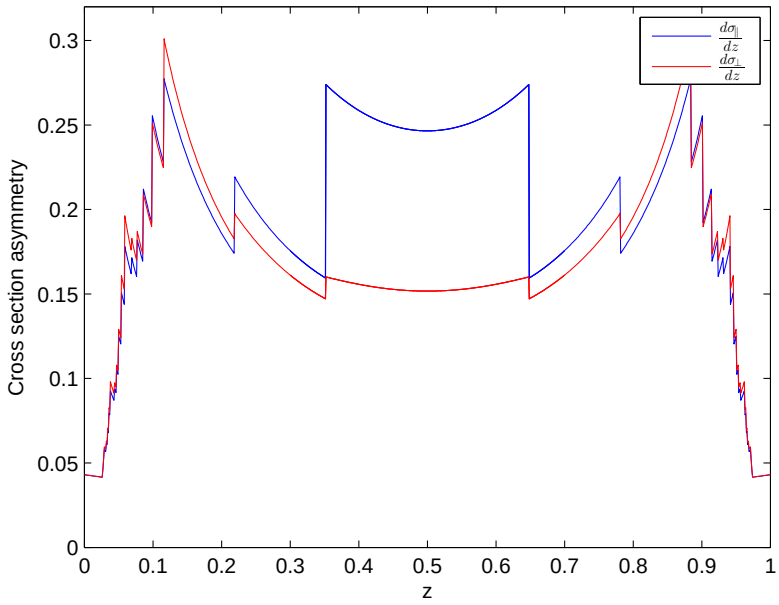

Fig. 1.2 Differential pair production inverse mean free path for Si at 132 GeV photon energy. $\theta = 1.4$mrad, $\alpha = 0.16$, where θ is the angle between the momentum of the incoming particle $\mathbf{p}_1$ and the [110] axis, and α is the angle between the plane containing $\mathbf{p}_1$ and the [110] axis with the plane containing the axes [001] and $[1\bar{1}0]$, see [10]

A plot of $\frac{d\sigma_\perp}{dz}$ and $\frac{d\sigma_\parallel}{dz}$, for 132 GeV incoming photons, can be seen in figure 1.2. The angles were chosen to achieve a significant asymmetry $\frac{d\sigma_\parallel - d\sigma_\perp}{d\sigma_\parallel + d\sigma_\perp}$ over the interval $0.3 < z < 0.7$ at a photon energy of 132 GeV.

Setting the degree of longitudinal polarization of the electron beam to zero $\lambda = 0$ and carrying out the entire calculation yields

$$\frac{d^3N_{\text{pairs}}}{dtdzdy} = \mathcal{L}_{e\gamma}\frac{d\sigma_c^{np}}{dy}\frac{I_i}{2\omega_i}\Big[\left(1 + \frac{2r^2}{f_1(y)}\cos^2\theta - \frac{f_3(y)}{f_1(y)}\Delta\sin\theta\right)\frac{1-q(y)}{\sigma_\perp(y)}\frac{d\sigma_\perp(y)}{dz} + \left(1 - \frac{2r^2}{f_1(y)}\cos^2\theta + \frac{f_3(y)}{f_1(y)}\Delta\sin\theta\right)\frac{1-r(y)}{\sigma_\parallel(y)}\frac{d\sigma_\parallel(y)}{dz}\Big] \tag{1.8}$$

where $y = \frac{\omega_f}{E}$ and E is the total electron energy and

$$f_1(y) = \frac{1}{1-y} + 1 - y - 4r(1-r), \tag{1.9}$$

$$f_2(y) = 2\lambda r x[1 + (1-y)(2r-1)^2], \tag{1.10}$$

$$f_3(y) = (1-2r)(\frac{1}{1-y} + 1 - y), \tag{1.11}$$

ω_f and ω_i are the photon energies after and before the scattering process, respectively and θ is the angle between the momentum of the incoming particle $\mathbf{p}_1$ and the [110] axis of the analyzer crystal.

The luminosity is given by

$$\mathcal{L}_{e\gamma} = 2N_e \int\int \rho_\gamma(\mathbf{x},t)\rho_e(\mathbf{x},t)d^3\mathbf{x}dt, \tag{1.12}$$

where $\rho_e(\mathbf{x},t)$ and $\rho_\gamma(\mathbf{x},t)$ are the unity normalized density profiles of the electron bunch and laser pulse, N_e is the number of electrons in the bunch, $r = \frac{y}{x(1-y)}$ with $x = \frac{4E\omega_i}{m^2}$ as above, λ is the degree of longitudinal polarization of the electron beam while

$$\frac{d\sigma_c^{np}}{dy} = \frac{2\pi\alpha^2}{xm^2} f_1(y), \tag{1.13}$$

$$\frac{d\sigma_1}{dy} = \frac{2\pi\alpha^2}{xm^2} rx(1-2r)(2-y), \tag{1.14}$$

and $\sigma_\parallel$ and $\sigma_\perp$ are the Compton scattering cross sections, as seen in [9].

1.3 Results

If we now consider $\theta = \omega_0 t$ and integrate over the whole energy interval $0 < y < y_m$ and integrate over a suitably chosen interval for z we get a pair-production rate. The Fourier transform of this rate has components at frequencies $\omega = 0$, $\omega = \omega_0$ and $\omega = 2\omega_0$. The component at $\omega = \omega_0$, selectable by tuning the frequency of the quarter-wave plate, is the one of interest. It is only present when the magnet is turned on, and thus signifies the effect of vacuum birefringence. The component at the double frequency is due to the fact that the polarization state of the Compton backscattered radiation depends on the initial polarization, and the polarizer crystal turns this into a difference in pair production rate.

In figure 1.3 is shown the result obtained for the `W`-stage of the FCC-ee, i.e. operation at 80 GeV. Even for a measurement as short as 3 hours, the peak arising from the change of polarisation in the magnetic field can be clearly identified.

In figure 1.4 is shown the result obtained for the `tt`-stage of the FCC-ee, i.e. operation at 175 GeV. Again, even for a measurement as short as 3 hours, the peak arising from the change of polarisation in the magnetic field can be clearly identified, and due mainly to the linear dependence of Δ on ω, equation (1.6), an even clearer signal is obtained at the highest energy.

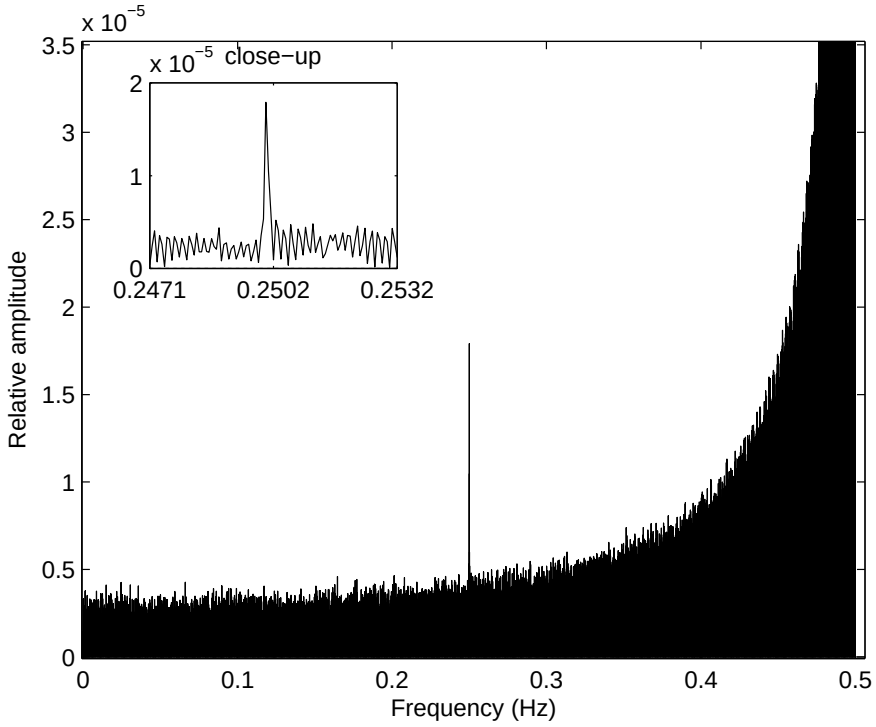

Fig. 1.3 The Fourier transform of the relative signal subtracted its average for the W-stage of the FCC-ee. The waveplate rotation frequency was here chosen as 0.25Hz. At the end of the spectrum the large component at the double frequency can be seen, while the main signal gives a distinct peak in the center, at the chosen frequency of the quarter-wave plate. The insert shows a close-up on the peak to display its narrow width, and clarity above background. This is for a 3 hour measurement.

1.4 Conclusion

We have shown that it is possible to measure the phenomenon of vacuum birefringence induced by a static magnetic field with high precision, within a quite short time frame, using Compton backscattered photons from the FCC-ee electron beam. Any outcome of such an experiment would be interesting. Either one would measure the QED vacuum birefringence for the first time or, in the case of an anomalous result, the experiment could point towards new physics, for instance the existence of the axion.

Acknowledgements UIU wishes to congratulate prof. W. Greiner on the occasion of his 80th birthday, and would like to thank for a very well-organized conference at the beautiful Makutsi, South Africa.

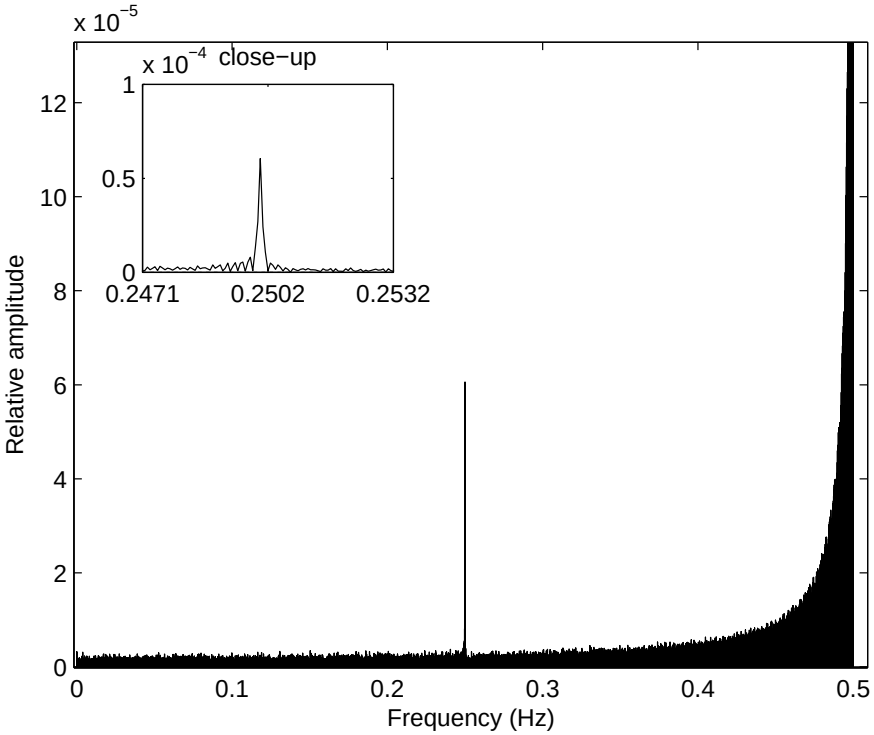

Fig. 1.4 The Fourier transform of the relative signal subtracted its average for the `tt`-stage of the FCC-ee. The waveplate rotation frequency was here chosen as 0.25Hz. At the end of the spectrum the large component at the double frequency can be seen, while the main signal gives a distinct peak in the center, at the chosen frequency of the quarter-wave plate. The insert shows a close-up on the peak to display its narrow width, and clarity above background. This is for a 3 hour measurement.

References

1. W. Heisenberg and H. Euler. Folgerungen aus der diracschen theorie des positrons. *Zeitschrift für Physik*, 98(11-12):714–732, 1936.
2. Julian Schwinger. On gauge invariance and vacuum polarization. *Phys. Rev.*, 82:664–679, Jun 1951.
3. John David Jackson. *Classical Electrodynamics*. John Wiley & Sons, Inc., New Jersey, USA, 3 edition, 1991.
4. Vladimir B Beresteckij, Evgenij M Lifsic, and Lev P Pitaevskij. *Quantum electrodynamics*. Butterworth-Heinemann, Oxford, 2008.
5. G.M. Shore. Superluminality and uv completion. *Nuclear Physics B*, 778(3):219 – 258, 2007.
6. M. Koratzinos. FCC-ee accelerator parameters, performance and limitations. *ArXiv e-prints*, November 2014.
7. Michael Bass. *Handbook of Optics: Volume I - Geometrical and Physical Optics, Polarized Light, Components and Instruments, Third Edition*. McGraw-Hill Professional:

New York, Chicago, San Francisco, Lisbon, London, Madrid, Mexico City, Milan, New Delhi, San Juan, Seoul, Singapore, Sydney, Toronto, 2010.
8. Tobias N. Wistisen and Ulrik I. Uggerhøj. Vacuum birefringence by compton backscattering through a strong field. *Phys. Rev. D*, 88:053009, Sep 2013.
9. I.F. Ginzburg, G.L. Kotkin, S.L. Panfil, V.G. Serbo, and V.I. Telnov. Colliding γe and $\gamma\gamma$ beams based on single-pass e^+e^- accelerators ii. polarization effects, monochromatization improvement. *Nuclear Instruments and Methods in Physics Research*, 219(1):5 – 24, 1984.
10. Mikhail Leonovich Ter-Mikaelian. *High-energy electromagnetic processes in condensed media*. Wiley-Interscience, 1972.